PCCP

ROYAL SOCIETY OF CHEMISTRY

PAPER

View Article Online
View Journal | View Issue

Cite this: *Phys. Chem. Chem. Phys.*, 2023, **25**, 6693

Role of the redox state of cerium oxide on glycine adsorption: an experimental and theoretical study†

Yuliia Kosto, ‡[a] Giovanni Barcaro, [b] Viacheslav Kalinovych, [a] Stefano Franchi, [c] Peter Matvija, [a] Iva Matolínová, [a] Kevin C. Prince, [c] Vladimír Matolín, [a] Tomáš Skála, [a] Nataliya Tsud *[a] and Vincenzo Carravetta [b]

Received 29th December 2022,
Accepted 6th February 2023

DOI: 10.1039/d2cp06068j

rsc.li/pccp

The role of the oxidation state of cerium cations in a thin oxide film in the adsorption, geometry, and thermal stability of glycine molecules was studied. The experimental study was performed for a submonolayer molecular coverage deposited in vacuum on CeO_2(111)/Cu(111) and Ce_2O_3(111)/Cu(111) films by photoelectron and soft X-ray absorption spectroscopies and supported by *ab initio* calculations for prediction of the adsorbate geometries, C 1s and N 1s core binding energies of glycine, and some possible products of the thermal decomposition. The molecules adsorbed on the oxide surfaces at 25 °C in the anionic form *via* the carboxylate oxygen atoms bound to cerium cations. A third bonding point through the amino group was observed for the glycine adlayers on CeO_2. In the course of stepwise annealing of the molecular adlayers on CeO_2 and Ce_2O_3, the surface chemistry and decomposition products were analyzed and found to relate to different reactivities of glycinate on Ce^{4+} and Ce^{3+} cations, observed as two dissociation channels *via* C–N and C–C bond scission, respectively. The oxidation state of cerium cations in the oxide was shown to be an important factor, which defines the properties, electronic structure, and thermal stability of the molecular adlayer.

Introduction

Knowledge of the physicochemical properties of small biological molecules adsorbed on a surface is essential for the development of novel knowledge-driven strategies in the fields of biomedical applications[1,2] and organic electronics.[3–5] The simplest proteinogenic amino acid glycine (NH_2–CH_2–COOH) is an example of a biomolecule with carboxylic acid and amino functional groups only (see Fig. 1). In addition to the important function of glycine as a building block of proteins in living organisms, its adsorption on metal or oxide films has applications in material functionalization for solar cells,[6] sensing systems for Cu^{2+}-ion detection,[7] and as a corrosion inhibitor.[8]

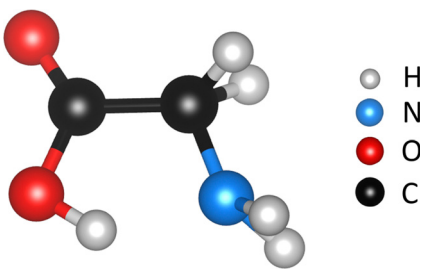

Fig. 1 Glycine (NH_2–CH_2–COOH) molecule. Light gray, blue, red, and black spheres correspond to hydrogen, nitrogen, oxygen, and carbon atoms, respectively.

Glycine is a classical model molecule for basic research in surface science due to its simple structure, stability, and similarity to other small bio- and organic molecules. The primary objective of model studies in a ultrahigh vacuum (UHV), in which molecules are deposited from the vapor phase on a substrate, is the characterization of the bonding of the molecule to a surface, with the aim to define the geometry, stability, and adsorption energy. Numerous studies of glycine adsorption on well-defined substrates have been published, including surfaces of metals[9–19] and oxides.[20–27] On Cu(111),[9,10,12] Cu(110),[13–17] and Cu(100),[12,17] independent of the surface

[a] *Charles University, Faculty of Mathematics and Physics, Department of Surface and Plasma Science, V Holešovičkách 2, Prague, 18000, Czech Republic. E-mail: Nataliya.Tsud@mff.cuni.cz*
[b] *Institute of Physical Chemical Processes-CNR, via Moruzzi 1, 56124 Pisa, Italy*
[c] *Elettra-Sincrotrone Trieste S.C.p.A., Area Science Park, Strada Statale 14, km 163.5, Basovizza (Trieste), 34149, Italy*

† Electronic supplementary information (ESI) available. See DOI: https://doi.org/10.1039/d2cp06068j

‡ Present address: Brandenburg University of Technology Cottbus-Senftenberg, Applied Physics and Semiconductor Spectroscopy, Konrad-Zuse-Strasse 1, 03046 Cottbus, Germany.

orientation, glycine undergoes deprotonation at 25 °C, adsorbing upright in a unidentate coordination at saturation coverage *via* one carboxylic oxygen accompanied by the formation of intermolecular hydrogen bonds. Annealing at 125 °C considerably changes the glycine adsorption geometry, in which bonding occurs *via* the two oxygen and the nitrogen atoms.[10,12,13] For the Pt(111) and Pd(111) surfaces, a saturation monolayer of glycine is formed by molecules in a zwitterionic[18,19] or neutral[11] phase, and bound *via* carboxylic and amino groups.

The glycine adlayer on the (110) and (011) surfaces of TiO_2 at 25 °C consists of zwitterionic ($^+NH_3$–CH_2–COO^-) and deprotonated (NH_2–CH_2–COO^-) species. The zwitterionic molecules are less stable and are converted to the deprotonated phase after annealing at temperatures of 50 °C and 175 °C, respectively.[20,21] The glycinate adlayer on TiO_2 is accommodated through two oxygens of the carboxylate group bridging two Ti atoms with the formation of an additional OH^- group.[20–22] Moreover, additional stabilization of the anionic molecule on TiO_2 could be expected through hydrogen bonding of the amino group to surface hydroxyl species.[22] Glycine's adsorption geometry on Al_2O_3/NiAl(110)[23] was shown to be similar to the case of TiO_2(110). DFT calculations of glycine adsorption on the Cr_2O_3(0001) surface[24] suggested the formation of the glycinate adlayer up to a saturation coverage through carboxyl and amino groups bound to surface Cr atoms. The molecules lie parallel to the surface at 0.25 monolayer (ML) coverage and bend upward at a coverage higher than 0.5 ML. In the case of Cr_2O_3(0001) functionalized with OH^- groups,[25] the glycine molecules adsorb mainly in the zwitterion form at low and saturation coverages.

In the present work, we employed oxidized CeO_2 and reduced Ce_2O_3 thin films as model substrates for glycine adsorption. Cerium oxide is a material with the ability to mimic the properties of several natural enzymes[28,29] and potentially can be used in a series of bioapplications[30] due to its ability to vary its oxidation state between Ce^{4+} and Ce^{3+} in response to environmental conditions. It was shown that cerium oxide could be used as a sensing electrode for the detection of glucose,[31] hydrogen peroxide,[32] cholesterol,[33] and in the treatments of Alzheimer's and Parkinson's diseases, cancer, diabetes, *etc.*[34–36] However, the interaction between the cerium oxide and living cells is not yet well understood. Thus, knowledge of the bioorganic–inorganic interface at different levels of complexity is of fundamental importance, in particular starting from the adsorption of the basic biological molecules on the surface of cerium oxide.

The model study on histidine bonding to cerium oxide films of different stoichiometries[37] and morphologies[38] is the most closely related work to the present research. On the well-ordered CeO_2(111) oxide, histidine deposited in UHV at 25 °C adsorbed *via* the deprotonated carboxylic group, the imino nitrogen atom of the imidazole (IM) ring, and the α-amino group. The deprotonation of the IM amino nitrogen was shown to be thermally activated and dependent on the surface concentration of the Ce^{4+} cations. An observed charge exchange between the histidine molecule and the oxide was related to the increased amount of the Ce^{3+} centers on the surface.[37] Later, it was shown that on the polycrystalline CeO_2 film,[38] histidine bound *via* the carboxylic acid group only, with the IM ring involved in the intermolecular hydrogen bonding.

Acetic acid adsorption and reactions on CeO_2(111) and CeO_x ($1.5 < x < 2$) oxide films[39] are other closely related systems. The formation of acetate adsorbed species together with surface hydroxyl groups was observed at 25 °C with further decomposition to mainly CO, CO_2, ketene, and water at elevated temperatures. Acetates on CeO_2(111) and CeO_x were stable up to 150 °C and 175 °C, respectively. Annealing at 425 °C stimulated complete desorption of the adsorbates from CeO_2(111) and left some residual carbon on CeO_x. C–O bond scission was proposed as an explanation for the CeO_x film reoxidation and formation of strongly adsorbed C_2H_x species, observed as a residual carbon signal.

The adsorption of formic acid and formate is also relevant to this study. It has been shown that the adsorption of formic acid with further thermal treatment does not influence the oxidation state of CeO_2(111). On partially reduced cerium oxide, however, it stimulates significant oxidation up to 125 °C and a reduction of the surface at higher temperature due to molecular decomposition.[40] The formic acid molecule decomposes preferably *via* dehydrogenation with the formation of CO_2 and H_2 on stoichiometric ceria film, while on the reduced CeO_x surface dehydration is favored with the formation of CO and H_2O.[41]

We present an experimental and theoretical study of glycine adsorption on ordered cerium oxide films of two stable stoichiometries—CeO_2(111) and Ce_2O_3(111)—by means of synchrotron radiation photoelectron spectroscopy (SRPES), X-ray photoelectron spectroscopy (XPS) with a laboratory source, resonant photoelectron spectroscopy (RPES), and near edge X-ray absorption fine structure spectroscopy (NEXAFS). Submonolayer glycine adlayers were deposited onto oxide films at 25 °C by evaporation in UHV. The glycine atoms' involvement in the interface formation on different oxides together with the thermal stability of the molecular adlayers were analyzed. *Ab initio* calculations were applied for prediction of the adsorbate geometry. The oxidation state of cerium cations in the oxide film was shown to play a role in the adsorption chemistry of glycine.

Experimental

SRPES, RPES, XPS, and NEXAFS

The experiments were performed at the Materials Science beamline at the Elettra synchrotron light source in Trieste, Italy. The experimental equipment consisted of a Specs Phoibos 150 hemispherical electron energy analyzer, an X-ray source with a Mg/Al dual anode, an e-beam evaporator filled with Ce, a gas inlet system, an ion gun, low energy electron diffraction (LEED) optics, a sample manipulator with a heating system and a K-type thermocouple attached to the rear side of the sample. The base pressure in the experimental chamber was 3×10^{-10} mbar.

The synchrotron light of the beamline was provided by a bending magnet and a plane grating monochromator, and was believed to be between 80–90% linearly polarized with a photon energy range of 22–1000 eV.

The Cu(111) single crystal (MaTecK, 8 mm diameter, 2 mm thickness) was used as a substrate for preparation of the cerium oxide thin films. The Cu crystal was cleaned by several cycles of Ar^+ ion sputtering with subsequent annealing at 500 °C until no C 1s or O 1s signal was observed in the photoelectron spectra. The CeO_2(111) thin film was prepared by e-beam physical vapor deposition of cerium (Goodfellow, 99.9% purity) in 5×10^{-7} mbar O_2 onto a Cu(111) substrate kept at 250 °C. After the deposition, the sample was annealed for 5 min at the same temperature and cooled under an oxygen atmosphere. The epitaxial (1×1) CeO_2(111)/Cu(111) thin film was confirmed by LEED. The thickness was estimated to be about 20.5 Å (corresponding to ~7 O–Ce–O layers) from the attenuation of the Cu $2p_{3/2}$ core level intensity measured by XPS.[42] The Ce_2O_3(111)/Cu(111) film was obtained by evaporation of metallic Ce on the CeO_2(111) buffer and subsequent annealing at 600 °C for 30 min. A 35.9 Å thick film with a (4×4) LEED pattern was obtained.[43] The film contained Ce cations in the 3+ oxidation state and the maximum concentration of oxygen vacancies.

Glycine powder (Alfa Aesar, 99.5% purity) was used without further purification. The deposition of glycine (30 s) was performed in the preparation chamber under vacuum (5×10^{-8} mbar) on the oxide surface at 25 °C using a home-made Knudsen-cell type evaporator. The glycine powder was degassed for 14 h. The temperature of the crucible with glycine molecules was about 90 °C during deposition.

The C 1s, N 1s, and O 1s core level spectra were acquired at photon energies of 410, 475, and 630 eV and total resolutions of 0.38, 0.49, and 0.69 eV, respectively. The intensity of the photoemission signal was then normalized to the incidence photon flux. The resolution was measured on Cu(111) as the width of the Fermi edge. The C 1s and N 1s core level spectra were fitted using a Voigt line shape with components of the same widths, after subtraction of the linear background. The Cu $2p_{3/2}$ and Ce 3d core level spectra were measured with the Al Kα anode of the laboratory X-ray source (total resolution 1 eV). The valence band spectra were measured at photon energy at and near resonance, namely 115, 121.4, and 124.8 eV, with a total resolution of 0.18 eV. This allowed us to obtain information about the Ce^{3+} and Ce^{4+} states in the topmost surface layer by characterization of the resonant Ce $4d \rightarrow 4f$ photoemission.[44] The valence band spectra acquired at 121.4 and 124.8 eV corresponded to D(Ce^{3+}) and D(Ce^{4+}) resonance enhancements of Ce^{3+} [binding energy (BE) 1.4 eV] and Ce^{4+} (BE 4 eV) ions, respectively (see Section S1 of the ESI† for details). The spectra measured at 115 eV corresponded to off-resonance for Ce^{3+} and Ce^{4+} states and were subtracted from the resonance spectra as a background. Information on the cerium chemical state, including the deeper layers of the film, was obtained from the analysis of the Ce 3d core level XPS spectra. The complex doublet structure of the Ce 3d core level represented different 4f configurations of cerium cations in the photoemission final state as a result of 4f orbital hybridization in the initial and final states.[45] The relative amounts of the Ce^{4+} and Ce^{3+} cations in the oxide were estimated from the areas of the components corresponding to the 4+ and 3+ oxidative states of cerium, determined after Ce 3d spectrum fitting carried out as in ref. 46 No radiation damage due to X-ray exposure was observed, as checked by changing the position of the analyzed spot on the sample surface.

NEXAFS spectra of glycine adsorbed on the cerium oxide surface were measured at the C and N K-edges using the partial KVV Auger electron yield acquisition mode. The spectra were acquired in two geometries: normal incidence, or NI (90°, with electric vector of the light parallel to the surface) and grazing incidence, or GI (10°, with electric vector of the light at 80° to the surface) of the photon beam to the sample. The energy resolution for the C and N K-edges were 0.23 and 0.38 eV, respectively. The raw spectra were normalized to the photon flux.

Glycine bonding and the adsorption structure on the cerium oxide films were characterized right after the deposition at 25 °C and after 1 min of annealing in UHV at 75, 100, 125, 150, 175, 200, and 250 °C. Since in this work we were studying non-saturated glycine adlayers, the molecular coverage was estimated considering the possibility of the molecular accumulation on the surface in the form of islands. For this purpose, the ratio of the N 1s intensity from glycine adlayers (after annealing at 75 °C) to the topmost surface part (about 3 Å[43]) of the Ce 3d signal acquired from the clean surface was analyzed (for details see Section S3 of the ESI†). We assume that the intensity of the N 1s peak derived from the 4 Å thick glycine islands of coverage θ. The topmost surface signal of the Ce 3d core level accounted directly for the uncovered part of the cerium oxide surface $(1 - \theta)$ and part of the surface covered by glycine (θ) with the Ce 3d intensity attenuated by the adlayer.[47] The values of glycine coverage for both cerium oxide films expressed in MLs are presented in Table 1. The estimated molecular coverages after glycine deposition were 0.11 and 0.09 ML for CeO_2 and Ce_2O_3, which means 1 glycine molecule per 9 and 11 Ce atoms, respectively.

Ab initio calculations

In order to provide a correlation between the core photoemission spectra collected on the two cerium oxide surfaces and the

Table 1 Molecular coverage of glycine θ_{Gly} (ML); binding energies E_b (eV) of the N 1s (component *A*) and C 1s (components *D*, *C*) core levels and the energy difference Δ (eV) between components *D* and *C* of the C 1s signal (Fig. 3)

Oxide film, temperature	θ_{Gly} (ML)	E_b (N 1s) (eV) component *A*	E_b(C 1s) (eV) components *D*, *C*	Δ (C 1s) (eV)
CeO_2(111) 75 °C	0.11	400.1 (*A*)	286.3 (*D*), 288.7 (*C*)	2.4
Ce_2O_3(111) 75 °C	0.09	401.5 (*A*)	288.0 (*D*), 290.4 (*C*)	2.4

nature of the adsorbate bonding, a theoretical investigation was carried out for simulation of the adsorption of glycine molecules and a number of different species, derived from glycine decomposition at higher temperatures, on CeO_2(111) and Ce_2O_3(111). The experimental conditions for the sub-monolayer adsorbate of glycine on a cerium oxide surface were simulated by a theoretical model system formed by a crystal slab and a single glycine molecule. The structure of the slabs included two planes of oxygen atoms and a plane of Ce atoms in the (111) orientation, for a total of 12 Ce atoms and 24 O atoms for CeO_2 and 16 Ce atoms and 24 O atoms for Ce_2O_3. The calculations concerned the identification of the main stable geometries of the different adsorbates in their electronic ground state, starting the optimization procedure from an average distance between the molecule and surface of about 5 Å and in a number of different molecular orientations suggested by previous studies of glycine on oxide surfaces.[20–22,26,27] Further calculations regarded the prediction of the binding energies of the C 1s and N 1s core levels of glycine and its fragments by using smaller model systems, including only the Ce and O atoms of the slab in closer contact with the adsorbed molecule in the adsorbate optimized geometries. For the optimization of the adsorbate geometry, the GAMESS program was used in the HF approximation, with the SBKJC effective core potential (ECP) for all Ce atoms, while the TZV basis set was adopted for the glycine atoms. The optimization of the adsorbate geometry was carried out by keeping the position of the slab atoms rigid, with the exception of the atoms directly interacting with the adsorbed molecule, in order to account for a possible reconstruction of the surface, which, however, turned out to be very modest. From the optimized geometries, smaller structures were cut, including the glycine or the fragments molecules and the slab atoms closest to the adsorbed species, for which the binding energies (BEs) of the C 1s and N 1s core levels were computed. Such calculations were carried out by the all electrons Hartree–Fock method, with the AhlrichsVTZ basis set for the adsorbed species and the CRENBL effective core potential for the slab atoms, using the DALTON program. This method neglects the smaller effect of the electronic correlation, but fully includes the electronic relaxation, which is the dominant effect in the ionization of the core shells.

Results

RPES, XPS

The oxidation state of the cerium cations in CeO_2 was estimated by analysis of the RPES valence band spectra, which contained Ce^{3+} and Ce^{4+} resonance features. The $D(Ce^{3+})/D(Ce^{4+})$ resonance enhancements ratio (RER) was estimated for the as-prepared CeO_2, and for the substrate after glycine deposition and after stepwise thermal treatment (Fig. 2a). After the deposition of glycine onto CeO_2 at 25 °C, the RER value changed from 0 to 0.1, which corresponded to about 2% of Ce^{3+} on the surface.[48] With the temperature increase, this rose to 0.4 and

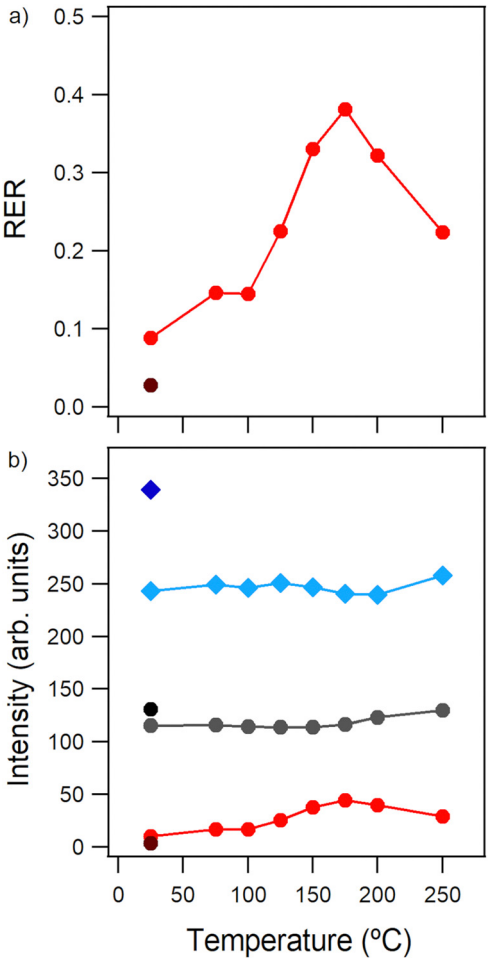

Fig. 2 (a) Resonant enhancement ratio calculated as $D(Ce^{3+})/D(Ce^{4+})$ *versus* the annealing temperature for glycine on CeO_2. Brown dot denotes the value for the clean CeO_2 surface. (b) Resonant enhancements of the $D(Ce^{3+})$ and $D(Ce^{4+})$ behaviors during the thermal treatment of glycine/CeO_2 (red and gray circles, respectively); and $D(Ce^{3+})$ for glycine/Ce_2O_3 (blue rectangles). The darker markers correspond to the values for the oxide surface before molecular adsorption.

then dropped to 0.2 after 175 °C and 250 °C, respectively. The RER values were not calculated for the Ce_2O_3 film, since there were no Ce^{4+} centers present in the film. However, the resonance enhancements $D(Ce^{3+})$ and $D(Ce^{4+})$ for CeO_2 and only $D(Ce^{3+})$ for Ce_2O_3 were analyzed for each surface and are shown in Fig. 2b. The behavior of $D(Ce^{3+})$ for CeO_2 *versus* the annealing temperature (Fig. 2b, red circles) reflected the RER behavior (Fig. 2a). It is worth noting that, together with the overall signal attenuation by the molecular adlayer, the decrease of $D(Ce^{4+})$ was accompanied by an increase of $D(Ce^{3+})$ to a comparable extent (Fig. 2b, gray and red circles), pointing to the partial surface reduction of Ce cations. This may be accounted for by water desorption or charge transfer from the molecule to the oxide. For Ce_2O_3, the decrease in $D(Ce^{3+})$ was much more pronounced after glycine deposition for a similar molecular coverage (Fig. 2b, blue rectangles), which indicated surface reoxidation. The $D(Ce^{3+})$ signal was stable during the annealing

series, with a slight increase after 250 °C. As for the Ce 3d core level, the adsorption of glycine did not induce any significant changes of the spectral shape. Analysis of the Ce 3d spectra revealed only a slight reduction of the CeO_2 surface and a partial reoxidation of the Ce_2O_3 film within the whole thickness after the last annealing step (Fig. S2, ESI†).

SRPES

The electronic structure and thermal stability of glycine adlayers on the oxide films were studied by analysis of the N 1s and C 1s core level spectra taken by SRPES. After molecular adsorption at 25 °C on both surfaces, one component (*A*) in the N 1s (Fig. 3a) and two components (*C* and *D*) in the C 1s spectra (Fig. 3b) were observed, with the spectral shape resembling the gas-phase molecular spectrum of glycine.[49] The energies of the components after annealing at 75 °C, when weakly bonded species desorbed, are presented in Table 1. In agreement with the literature, component *A* could be straightforwardly assigned to the core ionization of the nitrogen atom of the amino group,[18,23] while components *C* and *D* were assigned to carbon from the carboxylic group and to α-carbon connected to the amino group, respectively.[14,23] The BE of component *A* in the N 1s spectra on CeO_2 was in good agreement with the values published for adsorbed glycine with a neutral amino group.[18,21,50] The BE of the photoemission features for the adlayers on Ce_2O_3 was systematically higher than that for the glycine/CeO_2 system, which was attributed to the different band bending of the semiconducting oxide films.[40,51] The integral intensities of the N 1s and C 1s signals after annealing at each temperature are shown in Fig. 4a. The shape of the *C* and *D* components in the C 1s spectra was symmetrical, corresponding well to the two chemical states of carbon atoms. The energy difference between *C* and *D* was 2.4 eV on both oxides, smaller than the value of 2.9 eV for gaseous glycine[49,52] and glycine on Pt(111).[50] Thus, the strong bonding of the glycine molecule to the oxide surface substantially affected the separation of the C 1s components.

The existence of the neutral carboxylic group COOH in the molecule is often confirmed by the appearance of two features in the O 1s spectra separated in BE by 1.8–1.9 eV.[49,50,52] In the case of a glycine adlayer on the Pt(111) substrate, they were found at BEs of 531.4 and 533.3 eV.[50] In the current work, only one O 1s component at 531.8 eV was observed on CeO_2, besides

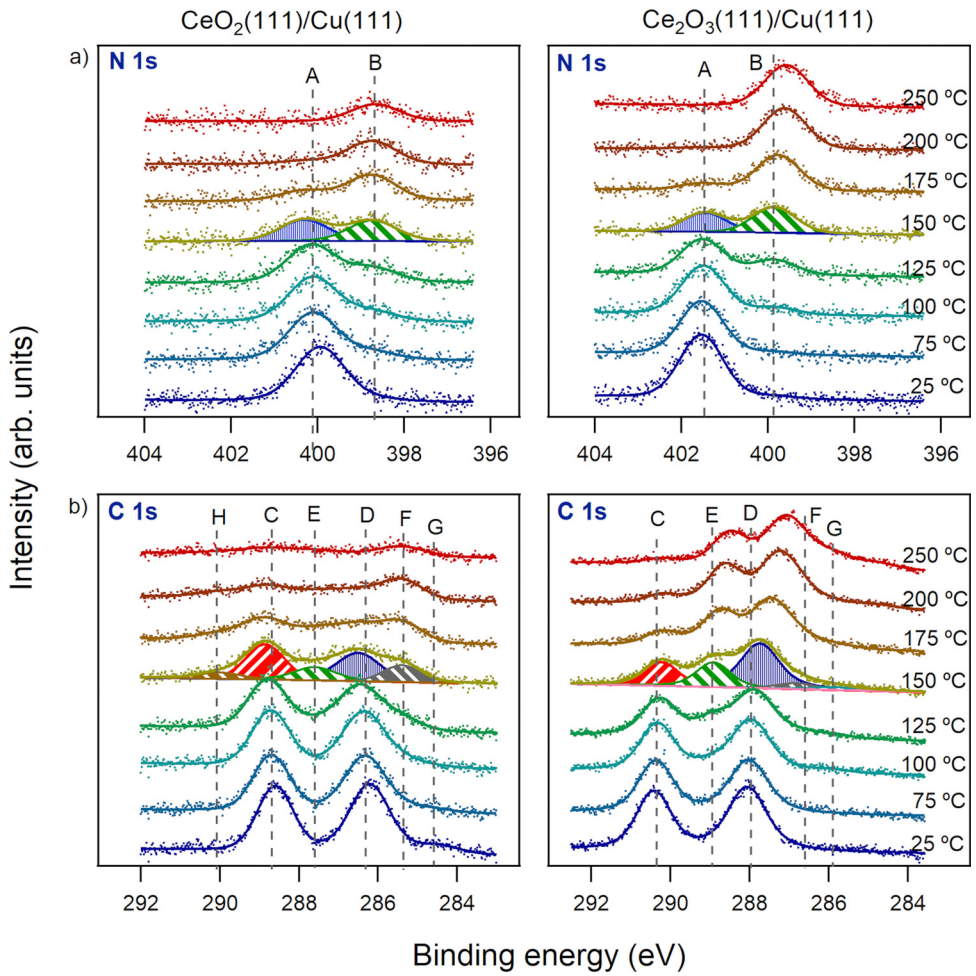

Fig. 3 N 1s (a) and C 1s (b) spectra of glycine adsorbed on CeO_2 (left column) and Ce_2O_3 (right column) surfaces. The temperature increased from 25 °C to 250 °C from the bottom to the top. The photon energies were 475 and 410 eV for N 1s and C 1s, respectively.

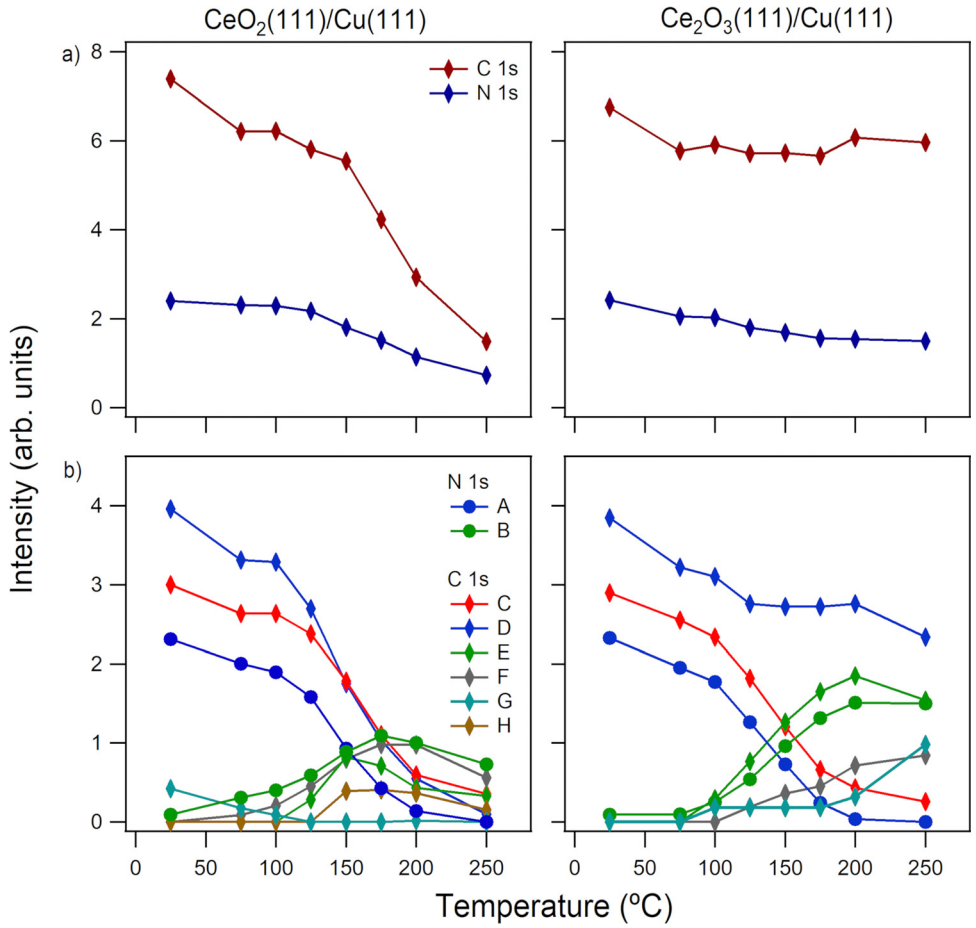

Fig. 4 (a) Integral intensities of the C 1s and N 1s peaks *versus* the annealing temperature for glycine on CeO_2 (left) and on Ce_2O_3 (right) surfaces and (b) thermal evolution of the separate features of the C 1s and N 1s spectra.

the lattice oxygen at 529.4 eV (Fig. 5, left), with the difference between their BEs being 2.4 eV. The signal at 531.8 eV was attributed to the carboxylate oxygen atoms of the glycine adlayer with a possible contribution of OH^- groups adsorbed on the Ce^{3+} cations formed as a result of partial oxide reduction. The O 1s spectrum of the clean Ce_2O_3 surface (Fig. 5, right) already contained a component at about 532.7 eV, which was assigned to the adsorbed OH^- groups on

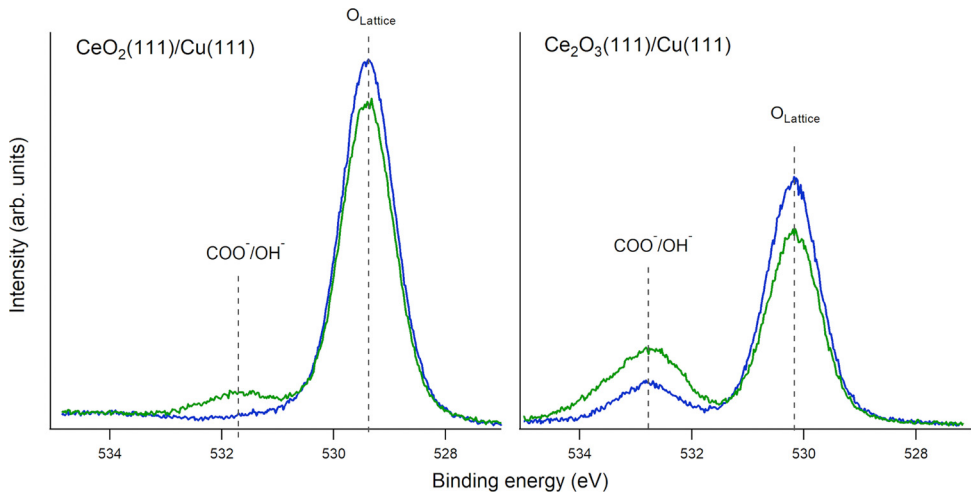

Fig. 5 O 1s spectra of glycine adsorbed on CeO_2 (left) and Ce_2O_3 (right) surfaces. The blue line corresponds to clean oxides and the green line corresponds to surfaces with glycine adlayers at 25 °C. Photon energy: 630 eV.

Ce^{3+} centers, with the lattice oxygen signal at 530.2 eV;[37] here, the difference between the components' BEs was 2.5 eV. After the deposition of glycine, attenuation of the lattice component was observed with a minor growth and broadening of the peak at 532.7 eV. We suggest that glycine was bonded to the surface of both oxides in a similar manner *via* deprotonated carboxylic groups.

Annealing of the systems at 75 °C did not change the shape of the spectra substantially, and only their integral intensity slightly dropped (Fig. 4a). The most prominent intensity decrease was observed for the C 1s of the glycine/CeO_2 system and could be explained by additional desorption of a small amount of contamination from the surface, as the low BE shoulder *G* has almost disappeared in Fig. 3b, left. On the Ce_2O_3 surface, apart from the reduced total intensity, no visible change of the spectra was observed (Fig. 4a, right). Further annealing showed different behaviors of the glycine adlayers on CeO_2 and Ce_2O_3 films. For CeO_2, the N 1s and C 1s intensities slowly decreased up to 150 °C, and then rapidly dropped after annealing at higher temperature. Interestingly, the C 1s signal decreased faster than the N 1s and could be tentatively linked to recombinative glycine desorption. On the Ce_2O_3 surface, the C 1s intensity remained almost unchanged after annealing at 75–250 °C, likely due to the high reactivity of the surface and strong interaction with the decomposition products. The N 1s intensity showed a slow linear decrease over the entire temperature range.

The behavior of the C 1s and N 1s components' intensity *versus* the annealing temperature is shown in Fig. 4b. For CeO_2, the intensity of the *A*, *C*, and *D* components slowly decreased up to 125 °C and then the slope of the curves became steeper (Fig. 4b, left). After annealing at 75–100 °C, a weak shoulder *F* appeared at about 285.5 eV with a simultaneous decrease of the *D* component. This could be tentatively explained by partial C–N bond splitting in glycinate with the formation of the adsorbed acetate (–CH_3 forms component *F* and the –COO^- group contributes to component C) and volatile ammonia.[53] This suggestion was also supported by Gong *et al.*,[54] who reported that oxidation of the Au(111) surface leads to dehydrogenation of the propylamines with further C–N bond cleavage. At low oxygen coverage, this decomposition channel was not activated, *i.e.*, only N–H bond splitting with the formation of propionitrile and water was observed.[54] Acetate was present as an intermediate species and rapidly transformed to the enolate $H_2C{=}HCO_{ads}$ adsorbates as a result of C–H and C–O bonds scission.[55] Component *F*, therefore, could be assigned to the adsorbed decomposition products with CH_3/CH_2 species and agreed well with the energy of the CH_3 peak of acetate on CeO_2(111)/Cu(111), as reported by Neitzel *et al.*[39] The signal from another carbon atom in acetate or an enolate group likely contributed to the intensity of component *C* or *E*, respectively. A new component *E* (287.6 eV) grew after annealing at 125 °C and then decreased after 150 °C, and was assigned to the CH_xO alkoxy-like or carbonyl species, as in ref. 39, 40 and 56 Traces of a low-BE peak *B* (398.7 eV) in the N 1s core level appeared already after 75 °C (Fig. 4b, left) and the peak was attributed to the partial dehydrogenation of the amino nitrogen of glycine engaged in the bonding to the surface. After treatment at higher temperature, components *B* and *E* behaved similarly. This could be interpreted as assuming C–C bond scission and the formation of adsorbed formate (initially contributing to component *C*, and then decomposing to a CH_xO-like species, forming component *E*) and imino species like –N=CH_2 (contributing to the C 1s component *D*, and forming the N 1s component *B*). However, this dissociation channel was less pronounced compared to the behavior of the spectroscopic features associated with the C–N bond cleavage. Annealing at higher temperatures led to a significant intensity drop and almost complete vanishing of the components *C* and *D*, and moreover components *A* and *C* behaved similarly throughout the annealing (Fig. 4b, left), which both supporting the idea of the recombinative desorption of glycine during the thermal treatment. Only residual carbon and nitrogen signals were left on the oxide surface after glycine decomposition and desorption.

On Ce_2O_3, annealing also led to a growth of component *B* (above 100 °C) in the N 1s spectra (Fig. 3a and 4b, right) simultaneously with component *E* in the C 1s spectra (Fig. 3b and 4b, right). As in the case of CeO_2, we suggest that these peaks were formed as a result of C–C bond cleavage and the formation of imino species, like –N=CH_2 (*B*) and formate (*C*), which then decomposed to adsorbed CH_xO (*E*). Peaks *B* and *E* were more pronounced on Ce_2O_3 than for the CeO_2 film, which could be assigned to the higher concentrations of surface Ce^{3+}. In contrast to glycine/CeO_2, the decrease in *C* correlated well with the rise of *E* in the C 1s spectra, confirming the change in the electronic environment of the carboxylate carbon atom. The decrease in *D* was slower and less than that for *C*, suggesting the strong bonding of –N=CH_2 to the oxide. Its intensity also remained stable in the temperature range 125–200 °C. Peak *F* (286.8 eV) appeared after 125 °C, attributed to the CH_3-containing species, for instance adsorbed acetate on Ce^{4+} centers. The weak peak *G*, identified after annealing at 100 °C, had a constant intensity up to 175 °C, and then rose. This could be assigned to adsorbed hydrocarbons CH_x, as a result of the surface reaction of the glycine adlayer at elevated temperature, or possibly to adventitious carbon. The shift of the peaks to lower BEs after annealing in the temperature range 150–250 °C (Fig. 3, right) was related to the change in the surface band bending due to the partial reoxidation of the film.

The ratios of the integrated intensities of the C 1s and N 1s core levels normalized to the photoionization cross-sections after annealing at 75 °C (see Fig. 4a) were 2.7 and 2.8 for glycine on the CeO_2 and Ce_2O_3 surfaces, respectively. Yet the theoretical value for the intact glycine molecule is 2. We suggest that such a difference could be caused by the specific adsorption geometry, at which the signals of C or N atom could be affected by the rest of the molecule or by carbon signal enhancement due to diffraction effects. For Ce_2O_3 with further annealing, the C : N ratio continuously rose to 4 after 250 °C. This confirmed the decomposition of the molecules and preferential desorption of the decomposition products with a higher N content. For CeO_2, this value remained quite stable and then after 175 °C decreased to 2, likely due to thermally induced surface chemical reactions in the glycinate adlayer.

NEXAFS

The NEXAFS spectra of glycine adsorbed on CeO_2 and Ce_2O_3 surfaces acquired after molecular deposition and after annealing at 175 °C are shown in Fig. 6. The positions of the peaks and their assignments are shown in Table 2. Comparing the NEXAFS data of glycine in thin films,[57,58] in powder,[59,60] or adsorbed on Cu(110),[14] the strong and narrow peak *R* in the C K-edge could be straightforwardly assigned to electron transition from the C 1s core level of the deprotonated carboxylic group to the lowest unoccupied orbital of π* symmetry. This peak was observed on both the studied model oxides. Similarly, the broad features *S* and *T* could be assigned to excitations of the 1s electrons to virtual orbitals of σ* symmetry localized on C–C, C–N, and C–O bonds, respectively.[57,59,60] For the as-deposited molecular adlayers, the angular dependence of the intensity ratio π*/σ*, *i.e.*, *R*/*S*, could be clearly observed in the C K-edge; here, peak *R* was stronger at GI for CeO_2 and at NI for Ce_2O_3, indicating that the carboxylic group of the glycinate was differently oriented on the two oxide films. The π* resonance intensity depends on the angle θ between the *E*-vector of the photons and the direction of the molecular orbital according to the equation $I \propto \cos^2\theta$.[61] Using this dependence, the tilt angle of the carboxylate group to the surface plane was estimated to be 32° and 48° on the CeO_2 and Ce_2O_3 oxides, respectively. After annealing at 175 °C, for CeO_2, a weak shoulder *R'* and a significant new peak *P* of π* character appeared at the low photon energy side. On Ce_2O_3, the peak *R'* became dominant and *P* was minor compared to the other features, in contrast to the case of CeO_2. We tentatively assigned the component *R'* to the adsorbed species with C=O bonds[41,62,63] and *P* to the enolate-like species with C=C bonds.[55,63] Such an assignment agreed well with the SRPES findings (Fig. 3).

In the N K-edge spectra at 25 °C, one prominent component *L* was observed. In agreement with previous publications, we assigned this peak to electron transition from the N 1s of the neutral amino group to virtual orbitals with an σ* character.[60,64] The weaker sharp features at 400–404 eV were assigned to the N 1s → σ* transitions.[14,65] Messer *et al.* also showed that such components appear only when the glycine amine moiety is present in a neutral configuration.[65] Since these features were visible in the case of glycine adsorbed on both CeO_2 and Ce_2O_3 films, we concluded that the amino group was neutral after the adsorption. However, these features were more pronounced on Ce_2O_3. Previously, it has been reported that the intensity of pre-edge N K-edge resonances could be substantially reduced, or indeed could vanish, if the amino nitrogen formed hydrogen bonds.[14,65] Thus, we suggest that there was a weak interaction of the glycine amino group with the CeO_2 surface through H-bonds after the deposition, which is a stronger bond than physisorption, and weaker than covalent bonding.

After the thermal treatment at 175 °C, an overall change of the spectral shape, with a strong π* resonance (*K*) and two broad σ* features (*L* and *M*), was observed and pointed to a change in the chemical environment of the amino nitrogen atom of glycine. A new sharp peak *K* at about 400 eV and a wide component *M* at 413 eV with an intensity similar to the feature *L* appeared in the spectra and were more prominent on Ce_2O_3. We suggest that peak *K* was due to the π* resonance of adsorbed imino-like species, like –N=CH_2,[66,67] which were formed as a result of C–C bond cleavage in glycinate, as concluded from the SRPES data above. This conclusion is in

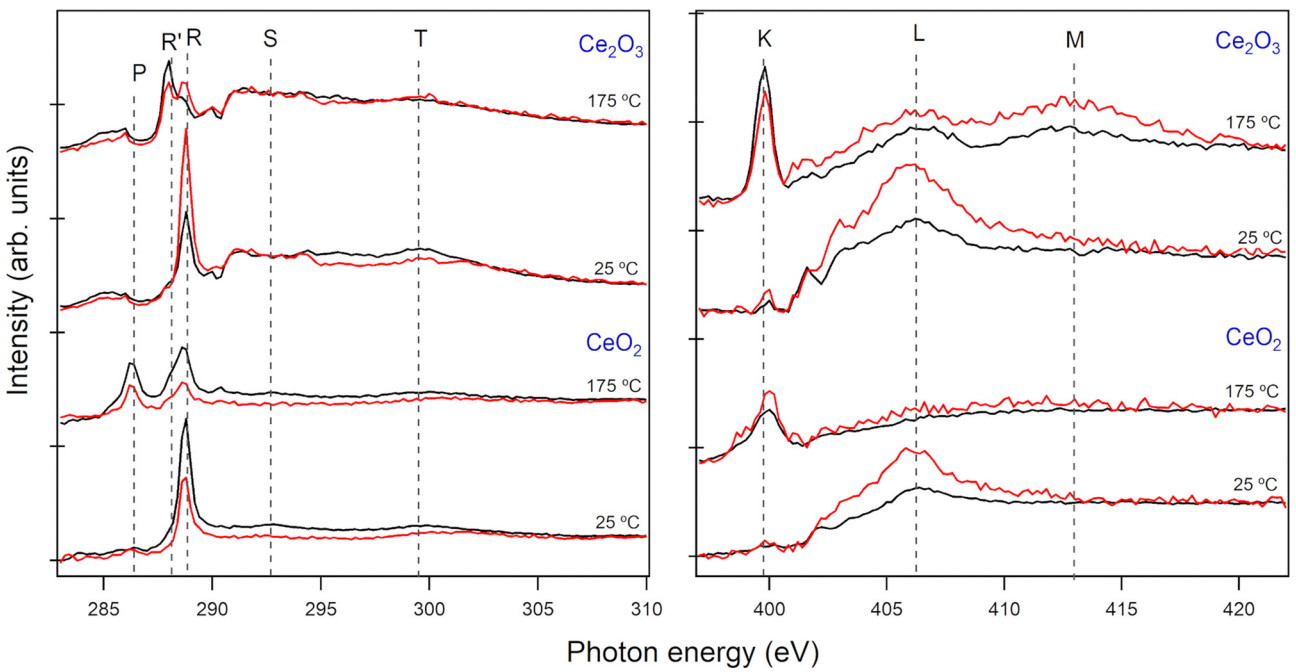

Fig. 6 NEXAFS C K-edge (left) and N K-edge (right) spectra of a glycine adlayer on CeO_2(111) and Ce_2O_3(111) surfaces recorded at 25 °C and after 1 min annealing at 175 °C. Black lines correspond to GI geometry, red lines to NI.

Table 2 Energy of the NEXAFS spectral components in eV and their assignment

	C K-edge	N K-edge
	C 1s → π* (C═C) (*P*) C 1s → π* (C═O, C═N) (*R'*), C 1s → π* (COO^-) (*R*), C 1s → σ* (C–C, C–N) (*S*) C 1s → σ* (C–O) (*T*)	N 1s → π* (C═N) (*K*), N 1s → σ* (C–N) (*L*) N 1s → σ* (C–N, C–H) (*M*)
Substrate		
CeO_2(111)	*P* *R'* *R* *S* *T*	*K* *L* *M*
temperature		
25 °C	—, —, 288.8, 292.0, 300.0	—, 406.2, —
175 °C	286.2, 288.0, 288.8, 292.0, 300.0	400.0, —, —
Ce_2O_3(111)		
temperature		
25 °C	—, —, 288.8, 292.0, 300.0	—, 406.0, —
175 °C	286.0, 288.0, 288.8, 292.0, 300.0	399.8, 406.4, 413.0

fair agreement with the work of Shavorskiy *et al.*,[66] in which the appearance of a sharp peak at about 400 eV in the N K-edge spectra of alanine on Cu(110) was suggested to be caused by decomposition of the molecules, specifically the dehydrogenation of methyl- and ethylamine intermediates and formation of (H_x)CN and CN species. The authors also showed that the dehydrogenation process depended on the density of oxygen atoms or hydroxyl groups on the substrate surface. Consequently, we tentatively attributed the *L* and *M* components to the virtual orbitals of σ* character of imino species adsorbed on the surface.[66]

Theoretical calculations

It is known that the glycine molecule, as well as other amino acids, strongly interacts with the surfaces of metal oxides through the carboxylic group, generally deprotonated, but a third anchor point can also be provided by the amino group. In order to identify the most stable forms of the glycine/cerium oxide adsorbate, energy optimization of some molecular structures was carried out at the HF level, using the SBKJC effective core potential for the slab atoms and the TZV basis set for the glycine atoms, as implemented in the GAMESS program. The optimized structures for the two adsorbates (GLY-ads1 and GLY-ads2) on the CeO_2(111) slab are shown in Fig. 7a and b. The first adsorbate had three anchor points provided by the interaction of three Ce atoms with the two oxygen atoms of the carboxylate group COO^- and the N atom of the amino group, while in the second case the amino group was not in contact with the surface. The interaction distances between the glycine atoms and the surface for the GLY-ads1 adsorbate were *R*(Ce–O) = 2.35 Å and *R*(Ce–N) = 2.65 Å, while for GLY-ads2 *R*(Ce–O) = 2.27 Å. These values indicate strong chemisorption. For the more extended interaction with the surface, the GLY-ads1 adsorbate was the most stable species at room temperature, while GLY-ads2 could be present on the surface in the case of high surface coverage (for steric reasons) or at higher temperatures. This latter aspect was relevant for analysis of the experimental spectra, which showed a significant dependence on the annealing temperature of the sample. On the other hand, increasing the temperature could lead to the dissociation of glycine with the formation of different fragments that can remain adsorbed on the surface in various conformations. Following suggestions in previous studies on the thermal decomposition of glycine powder[68] and glycine adsorbed on the Pt(111) surface,[50] as well as of acetic acid[39] adsorbed on the same CeO_2(111) surface, the adsorption geometry and the C 1s and N 1s core binding energies of six possible fragments were computed by the same approach adopted for the intact glycine molecule. The species considered were: formate ion ($HCOO^-$), acetate ion (CH_3COO^-), ketene (NH_2CHCO), methylamine (CH_3NH_2), formamide ($HCONH_2$), and CNH_2, which can be formed by breaking the C–C and C–N bonds of glycine. The adsorption geometries of such possible fragments on CeO_2(111) were energetically optimized as previously done for intact glycine. For all the fragments, the interaction distances for Ce–O, Ce–N, and Ce–C were in the range 2.3–3.0 Å, indicating the formation of stable chemisorbed species.

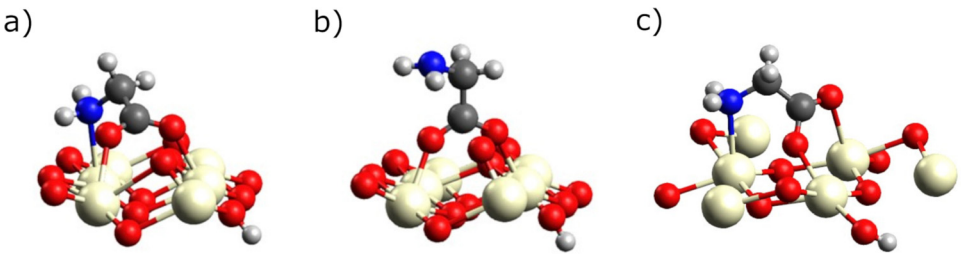

Fig. 7 Most stable geometries of glycine adsorbed on CeO_2(111): GLY-ads1 (a), GLY-ads2 (b); and on Ce_2O_3(111): GLY-ads1 (c).

Table 3 C 1s and N 1s ΔHF binding energies of the most stable adsorbates of glycine and its decomposition products on CeO_2(111) and Ce_2O_3(111) surfaces

	CeO_2(111)								Ce_2O_3(111)
	GLY ads1	GLY ads2	Formate $HCOO^-$	Acetate CH_3COO^-	Ketene NH_2CHCO	Methylamine CH_3NH_2	Formamide $HCONH_2$	CNH_2	GLY ads1
C(CN)	286.05	286.49				285.51		284.95	287.27
C(CH)				284.66	286.13				
C(CO)	288.70	289.28	288.60	288.37	288.83		289.06		288.70
N	400.10	399.97			400.40	399.59	400.56	401.51	400.96

The obtained theoretical BE values of the adsorbed glycine molecule and its decomposition products are reported in Table 3. These were not directly comparable to the experimental BEs, since the analyzer work function that affects the kinetic energy of the photoelectrons in photoemission measurements, estimated as 4.36 eV, was not considered in the calculations. In order to allow easier comparisons between the experimental spectra collected on CeO_2 and the theoretical BEs, all the computed BE values were shifted by −4.6 eV and −5.1 eV for the N 1s and C 1s core levels, respectively (Table 3), so that the position of the first band in the experimental spectrum and of the highest GLY-ads1 binding energy at the two 1s core levels were made to coincide. The same energy shifts were applied to the Ce_2O_3(111) case. The BE differences between the two theoretically predicted components of the C 1s signal were 2.6 and 2.8 eV for the ads1 and ads2 glycine adsorbates on CeO_2, respectively. The corresponding experimental value of 2.4 eV, together with the energy position of the components *C* (C 1s), *D* (C 1s), and *A* (N 1s) in Table 1, agreed well with the theoretically suggested glycine adsorption *via* two oxygen atoms and one nitrogen atom, *i.e.*, the ads1 geometry. The molecular coverage (about 0.1 ML) below saturation (about 0.25 ML) also confirmed that ads1 was the dominant adsorption mode of the glycine molecules on CeO_2 according to the considerations presented above. For the glycine bonding *via* three atoms to Ce_2O_3, the predicted BEs of the C 1s and N 1s components (Table 3) did not agree with the experimental values (Table 1), indicating that the adsorption geometry was different, as suggested above *via* only the carboxylic oxygen atoms. However, further stabilization of the glycinate molecule *via* the amino group attracted by the surface OH^- groups could not be excluded.

Discussion

In the current work, we used two substrates for investigation of glycine adlayers: stable CeO_2 and highly reactive Ce_2O_3 thin films, both grown on a Cu(111) single crystal. In CeO_2(111), the Ce cations are present predominantly in the 4+ state and each cation is coordinated to 8 oxygen anions. In Ce_2O_3(111), the Ce is present as Ce^{3+} cations that are bonded to 7 O^{2-}, with 3 oxygen anions closer and 4 further from Ce.[69] Thus, Ce_2O_3 differs from CeO_2 by the appearance of oxygen vacancies, with cerium cations in the 3+ oxidation state only. During the thermal treatment of glycine/cerium oxide systems, the most pronounced differences were between 25 °C and 175 °C, where also the NEXAFS spectra were taken. On both oxides, the as-deposited molecular adlayers were adsorbed *via* two carboxylic oxygen atoms in the anionic form, as was clearly demonstrated by analysis of the SRPES and NEXAFS results, and also as confirmed by *ab initio* calculations. Moreover, the optimal adsorption geometry of glycine on the CeO_2 film included a third adsorption point *via* the amino group. Also, during thermal treatment, the behavior of glycine on the CeO_2 and Ce_2O_3 films differed significantly.

In particular, the spectra collected at 25 °C on CeO_2 showed a single component *A* in the N 1s spectrum, two components *C* and *D* in the C 1s spectrum, a sharp π* resonance *R* in the C K-edge, and a broad σ* resonance *L* in the N K-edge NEXAFS spectrum, as expected from the electronic structure of glycinate adsorbed on an oxide surface. When increasing the temperature, the spectra showed a general decrease in intensity (Fig. 4a), but also, starting from 125 °C, the formation of new bands (*B* in N 1s, and *E*, *F*, *G* in C 1s) with lower BEs than the features observed at 25 °C. While the first trend could be reasonably attributed to an increasing recombinative desorption from the CeO_2 surface, the second could indicate the presence of different conformations of the adsorbed glycine, whose populations varied with the temperature, and alternatively or simultaneously, the appearance of fragments resulting from the glycine decomposition. The theoretical BEs are shown in Table 3 and, after comparison with the experimental results (Fig. 3), indicated that the formation of the component *B* at high temperatures could be partially correlated to the population of ads2, in which the amino group was not anchored to CeO_2, and which was less stable than ads1, but also to the formation of imino-like species. A similar analysis of the C 1s data (Fig. 3) and, in particular, of the *E* (CH_xO) and *F* (acetate) bands, the main components which appeared and partially replaced the *C* and *D* bands in the spectra above 125 °C, confirmed glycine decomposition on the CeO_2 surface. The π* resonances *K* in the N K-edge and *P* in C K-edge fully support the last conclusion. The possible presence on the surface of a minor amount of ads2 was indicated by band *H*, visible after annealing at 150 °C, and also based on the BE values provided by the calculations. Regarding the oxidation state of cerium cations on the CeO_2 surface, three temperature regions could be identified. First, at 25–100 °C, the surface reduction was connected with the glycinate adlayer adsorption and rearrangements. As for the histidine/CeO_2 system,[37] this reduction was likely

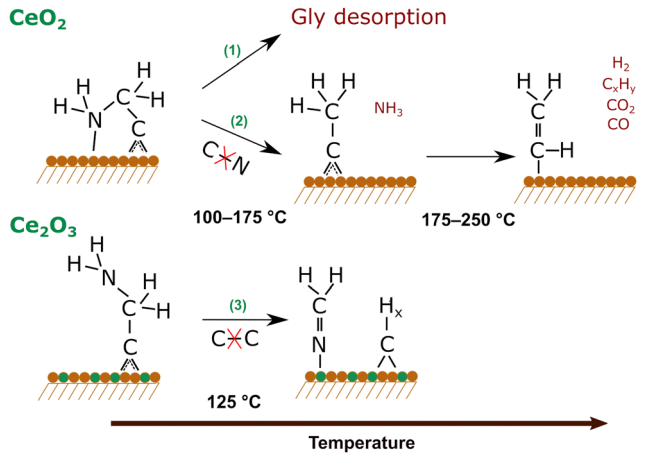

Fig. 8 Schematic illustration of the thermally stimulated glycine chemistry on CeO_2 and Ce_2O_3. Refer to the text for a detailed explanation.

to have an electronic character, as carboxylic oxygen atoms bind to the surface cerium cations (RER changed from 0 to 0.15), although minor water desorption from the surface could not be fully excluded. Further reduction in the range of 100–175 °C was connected with glycinate decomposition *via* the dehydrogenation and desorption of oxygen-containing species. In the last temperature region of 175–250 °C, surface oxidation was observed, confirming the recombinative desorption of glycine and dehydration of the surface species on the Ce^{3+} cations (the main decomposition channel for the glycinate on Ce_2O_3).

The photoemission spectra collected on Ce_2O_3 at 25 °C (Fig. 3, right) were similar to those collected on CeO_2, apart from a significant BE shift due to different bend bending. On Ce_2O_3, the formation of new bands (*B*, *E*, *F*, *G*) started after the annealing at 125 °C, but with different relative intensities with respect to those observed on CeO_2. Similar to the CeO_2 case, we could confirm the presence of formate, CH_xO, and imino-like species with the C=N double bond on Ce_2O_3, but in a more abundant form than on CeO_2, suggesting the easier decomposition of glycine on Ce_2O_3 *via* C–C bond scission. The features *R'* and *K* in the C and N K-edge NEXAFS, respectively, fully supported this conclusion. The minor component *F* after the annealing at 150 °C could be assigned to the acetate species, or to adsorbed CO as a decomposition product. The oxidation state of cerium cations on the surface did not change after glycinate adlayer formation at 25 °C, *i.e.*, all the carboxylate oxygen atoms of glycine filled the vacancy sites on the surface and glycinate decomposition was thus expected to proceed *via* the dehydrogenation and desorption of oxygen-free species. The small increase in the D(Ce^{3+}) states after annealing at 250 °C was attributed to thermally stimulated vacancy diffusion from the bulk to the surface,[43] as the Ce 3d core level showed higher oxidation state features within the whole oxide film.

A schematic illustration of the glycine adsorption chemistry on CeO_2(111) and Ce_2O_3(111) oxides together with the possible decomposition products is shown in Fig. 8. Summarizing the experimental findings, for the glycine adlyer on CeO_2(111), we observed: (1) the recombinative desorption of glycine starting from 125 °C, similarly to acetic acid on CeO_2.[55] Then, there were two other minor channels of glycine decomposition; (2) starting from 100 °C, C–N bond scission with the formation of acetate (components *C* and *F* in C 1s core level) and volatile NH_3. Further, acetate species likely underwent fast decomposition to enolate $H_2C{=}HCO$ type species (visible as component *P* in the C K-edge NEXAFS spectra at low photon energy). The observed glycinate dissociation on Ce^{4+} cations was in line with the recently reported deamidation activity of cerium oxide;[70] another channel (3) was connected to the C–C bond scission in glycine with the formation of formate (weak *R'* feature in the C K-edge NEXAFS and component *E* in the C 1s spectra) and imino-like $-N{=}CH_2$ species (weak *K* feature in the N K-edge NEXAFS and component *B* in the N 1s spectrum) on Ce^{3+} cations. This decomposition channel dominated for the glycine adlayer on the Ce_2O_3 oxide with some traces of channel (2) (when Ce^{4+} centers appear on the surface). There was an absence of the desorption of oxygenated species from Ce_2O_3, *i.e.*, all the oxygen atoms remained on the surface. Moreover, C–C bond scission resulted in the formation of carbonaceous deposits on the surface. Thus, the Ce_2O_3 surface turned out to be very reactive and remained covered by the glycine decomposition products after the final annealing, in agreement with the literature.[39,71] In turn, a negligible amount of the surface species remained on CeO_2 after the annealing at 250 °C, confirming the self-cleaning ability of the CeO_2, as also previously reported for the reaction with acetate.[39]

Conclusions

In the current work, we investigated glycine adlayers with low coverage of 0.11 and 0.09 ML on CeO_2(111)/Cu(111) and Ce_2O_3(111)/Cu(111) thin films, respectively. Molecules were deposited on the oxide substrates at 25 °C, and their thermal stability was studied upon stepwise annealing up to 250 °C. The results obtained from SRPES, RPES, and NEXAFS analysis and *ab initio* calculations showed that on both oxides, glycine molecules adsorbed in a deprotonated anionic state, bonding through the carboxylate group. Moreover, a third bonding point of glycine to CeO_2 was observed *via* the amino nitrogen group. In the course of the thermal treatment, glycine adlayers followed two different routes of decomposition, influenced by the type of cerium cations on the surface. Apart from recombinative desorption, the main decomposition path of glycine on the Ce^{4+} cations was *via* C–N bond scission, leading to formation of adsorbed acetate and volatile ammonia. The glycine decomposition on Ce^{3+} centers created by vacancies in the oxide film proceeded *via* C–C bond cleavage with the formation of formate, alkoxy, or carbonyl species and imino nitrogen groups with N=C double bond. The adsorbed species on the CeO_2 film decomposed first through dehydration and starting from 175 °C *via* dehydrogenation processes, leaving a negligible amount of the residual adsorbates on the surface after annealing at 250 °C. The surface chemistry of glycinate on Ce_2O_3 was

defined by the presence of vacancies in the oxide and proceeded mainly *via* dehydrogenation, forming strongly bound decomposition products on the oxide surface after 250 °C. The results supply additional information on the interaction of organic molecules with cerium oxide films, and can also contribute to the further development of novel systems for biomedical applications.

Author contributions

Y. Kosto and G. Barcaro: data curation, formal analysis, investigation, writing – original draft; V. Kalinovych, S, Franchi, P. Matvija: data curation, formal analysis; I. Matolínová and V. Matolín: funding acquisition, writing – review & editing; K. C. Prince: methodology, writing – review & editing; T. Skála: data curation, methodology, writing – review & editing; N. Tsud and V. Carravetta: conceptualization, investigation, methodology, supervision, writing – review & editing.

Conflicts of interest

There are no conflicts of interest to declare.

Acknowledgements

CERIC-ERIC consortium and Czech Ministry of Education, Youth and Sports (project LM2018116) are acknowledged for financial support.

References

1 V. Kalyanaraman, S. V. Naveen, N. Mohana, R. M. Balaje, K. R. Navaneethakrishnan, B. Brabu, S. S. Murugan and T. S. Kumaravel, Biocompatibility studies on cerium oxide nanoparticles-combined study for local effects, systemic toxicity and genotoxicity: Via implantation route, *Toxicol. Res.*, 2019, **8**, 25–37.

2 J. Lee, H. Byun, S. K. Madhurakkat Perikamana, S. Lee and H. Shin, Current Advances in Immunomodulatory Biomaterials for Bone Regeneration, *Adv. Healthcare Mater.*, 2018, **8**, 1801106.

3 S. J. Rodríguez and E. A. Albanesi, Electronic transport in a graphene single layer: Application in amino acid sensing, *Phys. Chem. Chem. Phys.*, 2019, **21**, 597–606.

4 C. Chen, M. Boota, P. Urbankowski, B. Anasori, L. Miao, J. Jiang and Y. Gogotsi, Effect of glycine functionalization of 2D titanium carbide (MXene) on charge storage, *J. Mater. Chem. A*, 2018, **6**, 4617–4622.

5 F. Ersan, O. Üzengi Aktürk, E. Aktürk and S. Ciraci, Metal-Insulator Transition and Heterostructure Formation by Glycines Self-Assembled on Defect-Patterned Graphene, *J. Phys. Chem. C*, 2018, **122**, 14598–14605.

6 F. Ersan, E. Aktürk and S. Ciraci, Glycine self-assembled on graphene enhances the solar absorbance performance, *Carbon N. Y.*, 2019, **143**, 329–334.

7 N. Ly, C. Seo and S.-W. Joo, Detection of Copper(II) Ions Using Glycine on Hydrazine-Adsorbed Gold Nanoparticles via Raman Spectroscopy, *Sensors*, 2016, **16**, 1785.

8 L. Chen, Y. He, Q. Yang, R. R. Yang, L. Zhang, Y. Fan and Z. He, A glycine derivative as corrosion inhibitor for carbon steel in 3.5 wt% NaCl solution: The combined experimental and theoretical calculation, *Int. J. Electrochem. Sci.*, 2018, **13**, 4640–4660.

9 D. A. Duncan, M. K. Bradley, W. Unterberger, D. Kreikemeyer-Lorenzo, T. J. Lerotholi, J. Robinson and D. P. Woodruff, Deprotonated Glycine on Cu(111): Quantitative Structure Determination by Energy-Scanned Photoelectron Diffraction, *J. Phys. Chem. C*, 2012, **116**, 9985–9995.

10 X. Zhao, H. Yan, R. G. Zhao and W. S. Yang, Self-Assembled Structures of Glycine on Cu(111), *Langmuir*, 2003, **19**, 809–813.

11 K. H. Ernst and K. Christmann, The interaction of glycine with a platinum (111) surface, *Surf. Sci.*, 1989, **224**, 277–310.

12 V. Efstathiou and D. P. Woodruff, Characterisation of the interaction of glycine with Cu(100) and Cu(111), *Surf. Sci.*, 2003, **531**, 304–318.

13 S. M. Barlow, K. J. Kitching, S. Haq and N. V. Richardson, A study of glycine adsorption on a Cu(110) surface using reflection absorption infrared spectroscopy, *Surf. Sci.*, 1998, **401**, 322–335.

14 J. Hasselström, O. Karis, M. Weinelt, N. Wassdahl, A. Nilsson, M. Nyberg, L. G. M. Pettersson, M. G. Samant and J. Stöhr, The adsorption structure of glycine adsorbed on Cu(110); comparison with formate and acetate, *Surf. Sci.*, 1998, **407**, 221–236.

15 M. Nyberg, J. Hasselström, O. Karis, N. Wassdahl, M. Weinelt, A. Nilsson and L. G. M. Pettersson, The electronic structure and surface chemistry of glycine adsorbed on Cu(110), *J. Chem. Phys.*, 2000, **112**, 5420.

16 N. A. Booth, D. P. Woodruff, O. Schaff, T. Giessel, R. Lindsay, P. Baumgärtel and A. M. Bradshaw, Determination of the local structure of glycine adsorbed on Cu(110), *Surf. Sci.*, 1998, **397**, 258–269.

17 J. W. Han, J. N. James and D. S. Sholl, Chemical speciation of adsorbed glycine on metal surfaces, *J. Chem. Phys.*, 2011, **135**, 34703.

18 P. Löfgren, A. Krozer, J. Lausmaa and B. Kasemo, Glycine on Pt(111): a TDS and XPS study, *Surf. Sci.*, 1997, **370**, 277–292.

19 F. Gao, Z. Li, Y. Wang, L. Burkholder and W. T. Tysoe, Chemistry of glycine on Pd(111): Temperature-programmed desorption and X-ray photoelectron spectroscopic study, *J. Phys. Chem. C*, 2007, **111**, 9981–9991.

20 T. J. Lerotholi, E. A. Kröger, M. J. Knight, W. Unterberger, K. Hogan, D. C. Jackson, C. L. A. Lamont and D. P. Woodruff, Adsorption structure of glycine on TiO_2(110): A photoelectron diffraction determination, *Surf. Sci.*, 2009, **603**, 2305–2311.

21 J. N. Wilson, R. M. Dowler and H. Idriss, Adsorption and reaction of glycine on the rutile TiO_2(011) single crystal surface, *Surf. Sci.*, 2011, **605**, 206–213.

22 R. Tonner, Adsorption of Proline and Glycine on the TiO_2(110) Surface: A Density Functional Theory Study, *Chem. Phys. Chem.*, 2010, **11**, 1053–1061.
23 G. Tzvetkov, G. Koller, Y. Zubavichus, O. Fuchs, M. B. Casu, C. Heske, E. Umbach, M. Grunze, M. G. Ramsey and F. P. Netzer, Bonding and structure of glycine on ordered Al_2O_3 film surfaces, *Langmuir*, 2004, **20**, 10551–10559.
24 P. A. Garrain, D. Costa and P. Marcus, Biomaterial-biomolecule interaction: DFT-D study of glycine adsorption on Cr_2O_3, *J. Phys. Chem. C*, 2011, **115**, 719–727.
25 D. Costa, P. Garrain, B. Diawara and P. Marcus, Biomolecule-biomaterial interaction: a DFT-D study of glycine adsorption and self-assembly on hydroxylated Cr_2O_3 surfaces, *Langmuir*, 2011, **27**, 2747–2760.
26 C. Li, S. Monti and V. Carravetta, Journey toward the Surface: How Glycine Adsorbs on Titania in Water Solution, *J. Phys. Chem. C*, 2012, **116**, 18318–18326.
27 G. Barcaro, L. Sementa, V. Carravetta, T. Yano, M. Hara and S. Monti, Experimental and theoretical elucidation of catalytic pathways in TiO_2-initiated prebiotic polymerization, *Phys. Chem. Chem. Phys.*, 2019, **21**, 5435–5447.
28 Y. Lin, J. Ren and X. Qu, Catalytically active nanomaterials: a promising candidate for artificial enzymes, *Acc. Chem. Res.*, 2014, **47**, 1097–1105.
29 X. Wang, Y. Hu and H. Wei, Nanozymes in bionanotechnology: from sensing to therapeutics and beyond, *Inorg. Chem. Front.*, 2016, **3**, 41–60.
30 F. Charbgoo, M. Bin Ahmad and M. Darroudi, Cerium oxide nanoparticles: green synthesis and biological applications, *Int. J. Nanomedicine*, 2017, **12**, 1401–1413.
31 M. Moumene, A. Tabet-Aoul, M. Gougis, D. Rochefort and M. Mohamedi, Laser pulse deposited nanosized ceria for direct electron transfer of glucose oxidase, *Int. J. Electrochem. Sci.*, 2014, **9**, 176–184.
32 Y. Kosto, A. Zanut, S. Franchi, Y. Yakovlev, I. Khalakhan, V. Matolín, K. C. Prince, G. Valenti, F. Paolucci and N. Tsud, Electrochemical activity of the polycrystalline cerium oxide films for hydrogen peroxide detection, *Appl. Surf. Sci.*, 2019, **488**, 351–359.
33 A. A. Ansari, A. Kaushik, P. R. Solanki and B. D. Malhotra, Sol-gel derived nanoporous cerium oxide film for application to cholesterol biosensor, *Electrochem. Commun.*, 2008, **10**, 1246–1249.
34 M. S. Wason and J. Zhao, Cerium oxide nanoparticles: potential applications for cancer and other diseases, *Am. J. Transl. Res.*, 2013, **5**, 126–131.
35 I. Celardo, J. Z. Pedersen, E. Traversa and L. Ghibelli, Pharmacological potential of cerium oxide nanoparticles, *Nanoscale*, 2011, **3**, 1411–1420.
36 C. K. Kim, T. Kim, I.-Y. Choi, M. Soh, D. Kim, Y.-J. Kim, H. Jang, H.-S. Yang, J. Y. Kim, H.-K. Park, S. P. Park, S. Park, T. Yu, B.-W. Yoon, S.-H. Lee and T. Hyeon, Ceria nanoparticles that can protect against ischemic stroke, *Angew. Chem., Int. Ed.*, 2012, **51**, 11039–11043.
37 N. Tsud, R. G. Acres, M. Iakhnenko, D. Mazur, K. C. Prince and V. Matolín, Bonding of histidine to cerium oxide, *J. Phys. Chem. B*, 2013, **117**, 9182–9193.
38 N. Tsud, S. Bercha, R. G. Acres, M. Vorokhta, I. Khalakhan, K. C. Prince and V. Matolin, Functionalization of nanostructured cerium oxide films with histidine, *Phys. Chem. Chem. Phys.*, 2015, **17**, 2770–2777.
39 A. Neitzel, Y. Lykhach, V. Johánek, N. Tsud, T. Skála, K. C. Prince, V. Matolín and J. Libuda, Decomposition of Acetic Acid on Model Pt/CeO_2 Catalysts: The Effect of Surface Crowding, *J. Phys. Chem. C*, 2015, **119**, 13721–13734.
40 Y. Lykhach, M. Happel, V. Johánek, T. Skála, F. Kollhoff, N. Tsud, F. Dvořák, K. C. Prince, V. Matolín and J. Libuda, Adsorption and Decomposition of Formic Acid on Model Ceria and Pt/Ceria Catalysts, *J. Phys. Chem. C*, 2013, **117**, 12483–12494.
41 S. D. Senanayake and D. R. Mullins, Redox Pathways for HCOOH Decomposition over CeO_2 Surfaces, *J. Phys. Chem. C*, 2008, **112**, 9744–9752.
42 F. Šutara, M. Cabala, L. Sedláček, T. Skála, M. Škoda, V. Matolín, K. C. Prince and V. Cháb, Epitaxial growth of continuous CeO_2(111) ultra-thin films on Cu(111), *Thin Solid Films*, 2008, **516**, 6120–6124.
43 T. Duchoň, F. Dvořák, M. Aulická, V. Stetsovych, M. Vorokhta, D. Mazur, K. Veltruská, T. Skála, J. Mysliveček, I. Matolínová and V. Matolín, Ordered Phases of Reduced Ceria As Epitaxial Films on Cu(111), *J. Phys. Chem. C*, 2014, **118**, 357–365.
44 V. Matolín, I. Matolínová, L. Sedlácek, K. C. Prince and T. Skála, A resonant photoemission applied to cerium oxide based nanocrystals, *Nanotechnology*, 2009, **20**, 215706.
45 A. Kotani and H. Ogasawara, Theory of core-level spectroscopy in actinide systems, *Phys. B*, 1993, **186–188**, 16–20.
46 T. Skála, F. Šutara, K. C. Prince and V. Matolín, Cerium oxide stoichiometry alteration via Sn deposition: Influence of temperature, *J. Electron Spectrosc. Relat. Phenom.*, 2009, **169**, 20–25.
47 R. G. Acres, X. Cheng, K. Beranová, S. Bercha, T. Skála, V. Matolín, Y. Xu, K. C. Prince and N. Tsud, An experimental and theoretical study of adenine adsorption on Au(111), *Phys. Chem. Chem. Phys.*, 2018, **20**, 4688–4698.
48 Y. Lykhach, S. M. Kozlov, T. Skala, A. Tovt, V. Stetsovych, N. Tsud, F. Dvorak, V. Johanek, A. Neitzel, J. Myslivecek, S. Fabris, V. Matolin, K. M. Neyman and J. Libuda, Counting electrons on supported nanoparticles, *Nat. Mater.*, 2016, **15**, 284–288.
49 O. Plekan, V. Feyer, R. Richter, M. Coreno, M. De Simone, K. C. Prince and V. Carravetta, Investigation of the amino acids glycine, proline, and methionine by photoemission spectroscopy, *J. Phys. Chem. A*, 2007, **111**, 10998–11005.
50 A. Shavorskiy, T. Eralp, K. Schulte, H. Bluhm and G. Held, Surface chemistry of glycine on Pt{111} in different aqueous environments, *Surf. Sci.*, 2013, **607**, 10–19.
51 S. Bercha, K. Beranová, R. G. Acres, M. Vorokhta, M. Dubau, I. Matolínová, T. Skála, K. C. Prince, V. Matolín and N. Tsud, Thermally Controlled Bonding of Adenine to Cerium Oxide: Effect of Substrate Stoichiometry, Morphology, Composition, and Molecular Deposition Technique, *J. Phys. Chem. C*, 2017, **121**, 25118–25131.

52 A. R. Slaughter and M. S. Banna, Core-photoelectron binding energies of gaseous glycine: correlation with its proton affinity and gas-phase acidity, *J. Phys. Chem.*, 1988, **92**, 2165–2167.
53 S. Bercha, S. Bhasker-Ranganath, X. Zheng, K. Beranová, M. Vorokhta, R. G. Acres, T. Skála, V. Matolín, K. C. Prince, Y. Xu and N. Tsud, Adsorption structure of adenine on cerium oxide, *Appl. Surf. Sci.*, 2020, **530**, 147257.
54 J. Gong, T. Yan and C. B. Mullins, Selective oxidation of propylamine to propionitrile and propionaldehyde on oxygen-covered gold, *Chem. Commun.*, 2009, 761–763.
55 F. C. Calaza, T.-L. Chen, D. R. Mullins, Y. Xu and S. H. Overbury, Reactivity and reaction intermediates for acetic acid adsorbed on CeO_2(111), *Catal. Today*, 2015, **253**, 65–76.
56 J. Zhou and D. R. Mullins, Adsorption and reaction of formaldehyde on thin-film cerium oxide, *Surf. Sci.*, 2006, **600**, 1540–1546.
57 V. Carravetta, O. Plashkevych and H. Ågren, A theoretical study of the near-edge X-ray absorption spectra of some larger amino acids, *J. Chem. Phys.*, 1998, **109**, 1456.
58 K. Kaznacheyev, A. Osanna, C. Jacobsen, O. Plashkevych, O. Vahtras, H. Ågren, V. Carravetta and A. P. Hitchcock, Innershell Absorption Spectroscopy of Amino Acids, *J. Phys. Chem. A*, 2002, **106**, 3153–3168.
59 Y. Zubavichus, A. Shaporenko, M. Grunze and M. Zharnikov, Innershell absorption spectroscopy of amino acids at all relevant absorption edges, *J. Phys. Chem. A*, 2005, **109**, 6998–7000.
60 Y. Zubavichus, M. Zharnikov, A. Schaporenko and M. Grunze, NEXAFS study of glycine and glycine-based oligopeptides, *J. Electron Spectrosc. Relat. Phenom.*, 2004, **134**, 25–33.
61 J. Stöhr, *NEXAFS Spectroscopy*, Springer, 1996.
62 P. A. Stevens, R. J. Madix and J. Stöhr, NEXAFS study of HCOO/Ag(110): Evidence for dynamic bending, *Surf. Sci.*, 1990, **230**, 1–12.
63 D. A. Outka, J. Stöhr, R. J. Madix, H. H. Rotermund, B. Hermsmeier and J. Solomon, NEXAFS studies of complex alcohols and carboxylic acids on the Si(111)(7 × 7) surface, *Surf. Sci.*, 1987, **185**, 53–74.
64 E. Otero and S. G. Urquhart, Nitrogen 1s Near-Edge X-ray Absorption Fine Structure Spectroscopy of Amino Acids: Resolving Zwitterionic Effects, *J. Phys. Chem. A*, 2006, **110**, 12121–12128.
65 B. M. Messer, C. D. Cappa, J. D. Smith, K. R. Wilson, M. K. Gilles, R. C. Cohen and R. J. Saykally, pH Dependence of the Electronic Structure of Glycine, *J. Phys. Chem. B*, 2005, **109**, 5375–5382.
66 A. Shavorskiy, F. Aksoy, M. E. Grass, Z. Liu, H. Bluhm and G. Held, A step toward the wet surface chemistry of glycine and alanine on Cu{110}: destabilization and decomposition in the presence of near-ambient water vapor, *J. Am. Chem. Soc.*, 2011, **133**, 6659–6667.
67 H. Yabuta, M. Uesugi, H. Naraoka, M. Ito, A. L. D. Kilcoyne, S. A. Sandford, F. Kitajima, H. Mita, Y. Takano, T. Yada, Y. Karouji, Y. Ishibashi, T. Okada and M. Abe, X-ray absorption near edge structure spectroscopic study of Hayabusa category 3 carbonaceous particles, *Earth, Planets Sp.*, 2014, **66**, 156.
68 V. Y. Yablokov, I. L. Smel'tsova, I. A. Zelyaev and S. V. Mitrofanova, Studies of the rates of thermal decomposition of glycine, alanine, and serine, *Russ. J. Gen. Chem.*, 2009, **79**, 1704–1706.
69 D. R. Mullins, The surface chemistry of cerium oxide, *Surf. Sci. Rep.*, 2015, **70**, 42–85.
70 S. Bhasker-Ranganath and Y. Xu, Hydrolysis of Acetamide on Low-Index CeO_2 Surfaces: Ceria as a Deamidation and General De-esterification Catalyst, *ACS Catal.*, 2022, **12**, 10222–10234.
71 D. R. Mullins and P. M. Albrecht, Acetaldehyde Adsorption and Reaction on CeO_2(100) Thin Films, *J. Phys. Chem. C*, 2013, **117**, 14692–14700.

